Supplementary Materials

Visualizing Magnetic Structure in 3D Nanoscale Ni-Fe Gyroid Networks

Justin Llandro[1,2,3]*, David M. Love[4], Andras Kovács[5], Jan Caron[5], Kunal N. Vyas[4]‡, Attila Kákay[6], Ruslan Salikhov[6], Kilian Lenz[6], Jürgen Fassbender[6,7], Maik R. J. Scherer[4]§, Christian Cimorra[4], Ullrich Steiner[8], Crispin H. W. Barnes[4], Rafal E. Dunin-Borkowski[5], Shunsuke Fukami[1,2,3] and Hideo Ohno[1,2,3].

[1]Laboratory for Nanoelectronics and Spintronics, Research Institute of Electrical Communication, Tohoku University, 2-1-1 Katahira, Aoba-ku, Sendai 980-8577, Japan.

[2]Center for Spintronics Research Network, Tohoku University, 2-1-1 Katahira, Aoba-ku, Sendai 980-8577, Japan.

[3]Center for Science and Innovation in Spintronics (Core Research Cluster), Tohoku University, 2-1-1 Katahira, Aoba-ku, Sendai 980-8577, Japan.

[4]Department of Physics, Cavendish Laboratory, University of Cambridge, J.J. Thomson Avenue, Cambridge CB30HE, United Kingdom.

[5]Ernst Ruska-Centre for Microscopy and Spectroscopy with Electrons (ER-C), Forschungszentrum Jülich, 52425 Jülich, Germany.

[6]Helmholtz-Zentrum Dresden - Rossendorf (HZDR), Bautzner Landstrasse 400, 01328 Dresden, Germany.

[7]Technische Universität Dresden, Haeckelstrasse 3, 01069 Dresden, Germany.

[8]Adolphe Merkle Institute, Chemin des Verdiers 4, 1700 Fribourg, Switzerland.

[9]Center for Innovative Integrated Electronic Systems (CIES), Tohoku University, 468-1 Aramaki Aza Aoba, Aoba-ku, Sendai 980-0845 Japan.

[10]WPI Advanced Institute for Materials Research (WPI-AIMR), Tohoku University, 2-1-1 Katahira, Aoba-ku, Sendai 980-8577, Japan.

‡Present address: Lightpoint Medical Ltd., Misbourne Works, Waterside, Chesham HP51PE, UK.
§Present address: Papierfabrik Louisenthal GmbH, 83701 Gmund am Tegernsee, Germany.

1. High-symmetry directions of the single-gyroid network

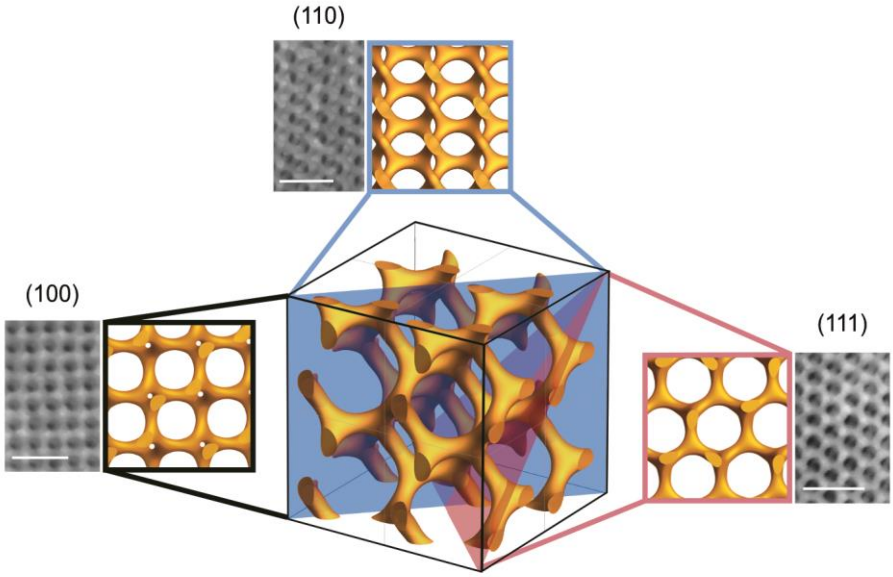

Figure S1. Schematic of 2×2×2 unit cells of a single-gyroid network with volume fraction 20%, showing the (100) (black line), (110) (blue line) and (111) (red line) faces with corresponding SEM images of well-ordered gyroid films. Scale bars are 100 nm.

2. Materials and Methods

(a) Preparation of block co-polymer gyroid templates:

The di-block co-polymer (BCP) used in this study is poly(4-fluorostyrene)-b-poly(D,L-lactide) (PFS-b-PLA, MW = 24 kg · mol^{-1}) with a 38 vol % PLA fraction.[1] Three types of samples were made: for transmission electron microscopy (TEM) analysis on fluorine-doped tin oxide (FTO)-coated glass, for electron holography (EH) on TEM grids and for bulk magnetometry on Au-coated Si substrates. To prepare samples for TEM analysis, firstly fluorine-doped tin oxide (FTO) coated glass substrates (Solaronix) were cleaned for 15 minutes at 80 °C in a strong piranha solution, containing three parts sulfuric acid (laboratory reagent grade, 95 %, Fisher Scientific) and one part hydrogen peroxide (puriss, 30 %, Sigma Aldrich). Then, the substrates were treated with octyltrichlorosilane[1] and a BCP film approximately 1 μm thick was prepared by spin-coating a 10 wt % solution of the polymer in toluene onto the substrates at 200 rpm. The samples were then heated under vacuum at a ramp rate of 2.5 °C/min until reaching the annealing temperature of 173 °C and annealed for 20 min under a nitrogen atmosphere, during which time the polymer anneals into the double gyroid morphology. After quenching the samples to room temperature, they were immersed in 0.1M aqueous sodium hydroxide solution containing 50 wt % methanol for several hours during which the removal of the PLA minority phase took place. The double-gyroid PFS templates were then washed in methanol and dried in a nitrogen stream.

For EH samples, FTO substrates were prepared as above but without silanization in order to keep the surface hydrophilic. Copper TEM grids coated with a bi-layer of "lacey" carbon and graphene oxide (Agar Scientific AGS166-4H-GO) were then placed on the spun BCP film, spread with 10 μL of the BCP solution using a pipette tip and spun again as before. During the PLA removal step, the TEM grids were released from the hydrophilic FTO-glass substrates, washed in methanol and carefully dried in a nitrogen stream, as above.

To prepare samples for bulk magnetometry, the Au-coated Si substrates were masked with a photoresist template to define a 1 mm diameter circle for the subsequent electro-deposition step. They were then spin-coated with the BCP film and thermally annealed as described above.

(b) Electrodeposition of Ni-Fe into PFS gyroid templates and composition analysis: Electrodeposition of Ni-Fe was performed in a standard three-electrode electrochemical cell with a polished stainless steel counter electrode and an Ag/AgCl working electrode using an Autolab potentiostat (PGSTAT302N, Metrohm). A sharpened pair of stainless steel tweezers provided the electrical connection to a small area of the conductive substrate from which the PFS film had been removed. The Ni-Fe plating solution was prepared by mixing 2.4732 g boric acid, 1.7761 g nickel (II) sulfamate tetrahydrate (formula weight 322.93), 305.811 mg iron (II) sulfate heptahydrate (formula weight 278.01) and 274.77 mg saccharin (all from Sigma Aldrich) into 100 mg of ultrapure water (MilliQ, Merck Millipore, 18.2 MΩ · cm). The pH of the solution was adjusted to 3.0 by micro-pipetting very small amounts of either NaOH or ammonia. The solution was heated to 50 °C and the PFS-coated substrates were dipped in methanol to allow the aqueous electrolyte to infiltrate the hydrophobic PFS template before immersing them in the plating solution. For TEM grid samples, a nucleation pulse of -2.0 V was initially applied for 0.5 s to seed the grid surface with a low density of metal nanoclusters in order to preferentially nucleate the gyroid growth in random, well-separated areas, followed by uniform Ni-Fe electrodeposition into the templates under a constant potential of -1.55 V while the deposited charge was monitored. For the samples on FTO and Si/Au, 25 mC was deposited, after which the samples were immediately rinsed in deionized water and dried with nitrogen. For the TEM grids, two sets of samples were grown with deposited charges of 20 mC and 5 mC, respectively. After rinsing with deionised water, the TEM grids were immersed in toluene to remove the PFS template; this was not done on the Si/Au samples due to the photoresist mask. Scanning electron microscopy of the TEM grid samples revealed the growth of dense double-gyroid nanoparticles on both sides of the grids on the 20 mC sample and both single-gyroid and double-gyroid nanoparticles on the 5 mC sample. Composition analysis of the electrodeposited Ni-Fe by energy-dispersive X-ray spectroscopy (EDX) showed very low levels of contaminants from the electrodeposition solution and a composition of $Ni_{75}Fe_{25}$.

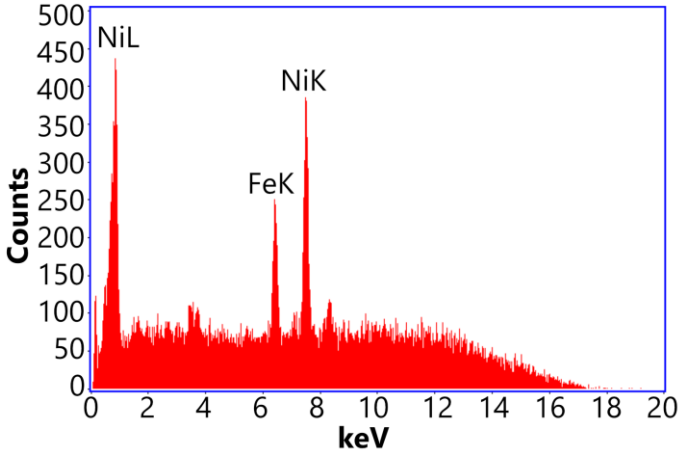

Figure S2. Energy-dispersive X-ray spectroscopy (EDX) of electrodeposited Ni-Fe gyroid film samples, showing that the films have very low levels of incorporated contaminants from the electrodeposition solution. Peak analysis gives a composition for the film of 74.28 at. % (75.23 wt. %) Ni and 25.72 at. % (24.77 wt. %) Fe.

(c) Off-axis electron holography:
Transmission electron microscopy (TEM) was carried out in an FEI Titan 80-300 XFEG electron microscope operated at 300 kV.[2] For magnetic imaging, the specimen was placed in magnetic-field-free conditions (Lorentz mode) with the conventional objective lens turned off and using an aberration corrector unit to improve the spatial resolution. The excitation of the objective lens was varied to apply magnetic fields to the specimen up to 1.4 T. In off-axis electron holography experiments, the biprism voltage was typically set to 120 V to produce an overlap interference width of 600 nm and a holographic interference fringe spacing of 2.6 nm with a contrast of 20%. Electron holograms were recorded using a 2048×2048 pixel conventional charge coupled-device (CCD) camera with a typical exposure time of 8 s. Off-axis electron holograms were reconstructed numerically using a standard Fourier transform based method with sideband filtering using customized SEMPER[3] software. Contour lines and color maps were generated from recorded magnetic phase images to yield magnetic induction maps.

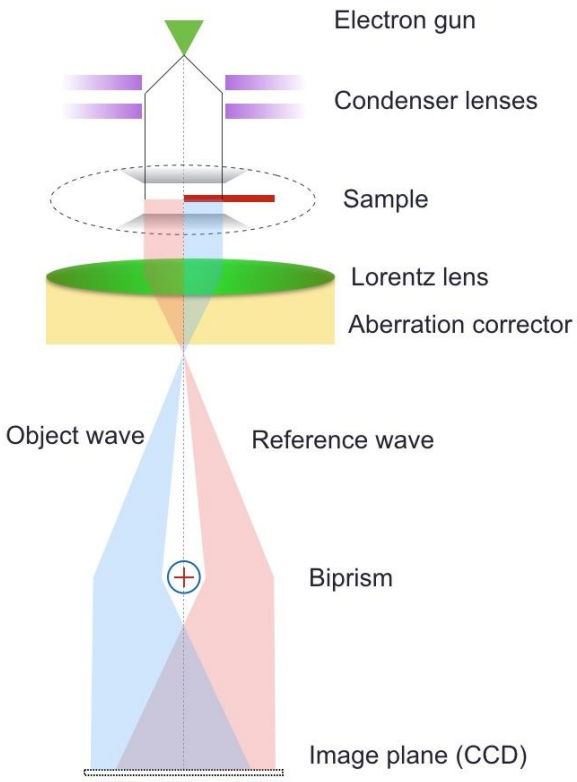

Figure S3. Schematic figure of the ray path of off-axis electron holography. A highly coherent electron wave is passing through the sample that is positioned in magnetic-field-free conditions. The electrons are focused and controlled by a Lorentz lens. The lens aberrations are reduced by the aberration corrector. The part of the electron wave that passes through vacuum is used as the reference wave. The object wave contains the phase information. A positively charged biprism is used to obtain the electron hologram, which is recorded by a CCD detector. The holograms are processed with SEMPER computer software.[3]

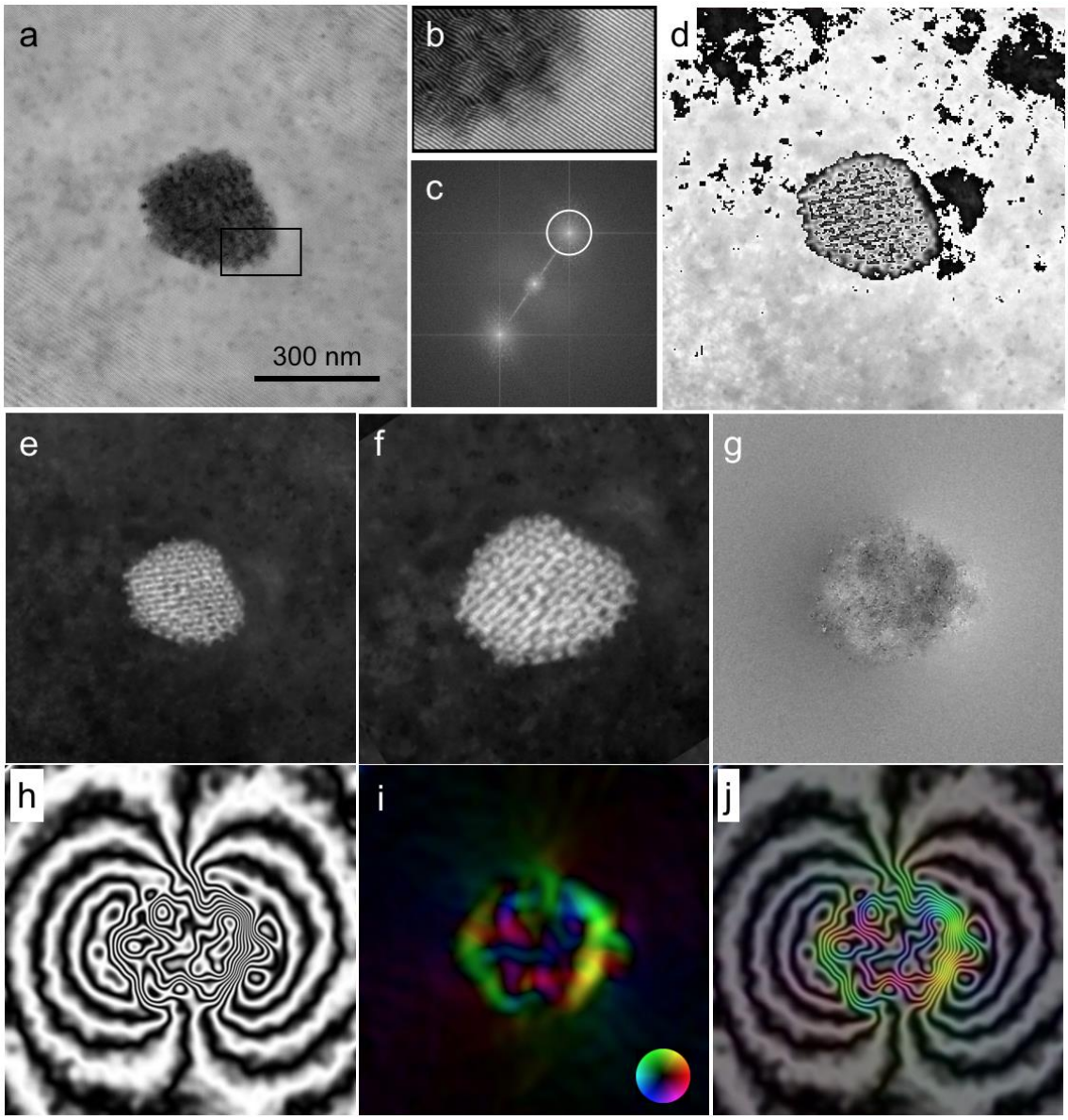

Figure S4. Processing steps of electron holograms. (a) An electron hologram of the double-gyroid nanoparticle shown in Figure 4 of the main text. (b) The enlarged region from (a) showing the fringes and the electromagnetic field induced changes at the double-gyroid edges. (c) Fourier transform of the hologram containing a center band and two sidebands. One of the sidebands is selected and an inverse Fourier transform is applied. (d) Wrapped phase image containing phase discontinuities. (e) Unwrapped total phase. Two total phase maps were recorded by applying magnetic fields from antiparallel directions. (f) Mean inner potential map obtained by taking half the sum of the total phase images. (g) Magnetic phase image obtained by taking half the difference of the two total phase images. (h) Magnetic phase contours (spacing $2\pi/64$ radians) corresponding to the cosine of 64 times the phase image shown in (g). (i) Color map derived from the gradient of the magnetic contribution to the phase shift. The hue and intensity of the colors are used to label the direction and magnitude, respectively, of the in-plane component of the projected magnetic induction. (j) Magnetic phase contours and color map added to each other.

Although we focus on small nanoparticles to observe the details of the gyroids' magnetization distribution, useful information can be gained from larger structures such as double-gyroid "nanowires" produced by heterogeneous nucleation at the border of graphene oxide and carbon (**Figure S5**). The width of this nanowire is approximately 150 nm while the length is several microns. The magnetic induction map extracted from EH measurements shows that the field lines follow the main axis of the nanowire and exit at the ends in the same fashion as a bar magnet. Inside the body the field distribution produces a small angle variation due to the formation of magnetic domains with size of a few tens of nanometers. The change of the external saturating magnetic field (~1.4 T) direction switches the field direction within the wire and introduces only a small rearrangement of the magnetic domains. The field distribution resembles a ferromagnetic nanowire, although the measured step in the magnetic phase across the middle of the double-gyroid nanowire is 3.8 radians, which is much weaker than that which a solid permalloy nanowire would produce (approximately 37.8 radians), confirming a porous structure.

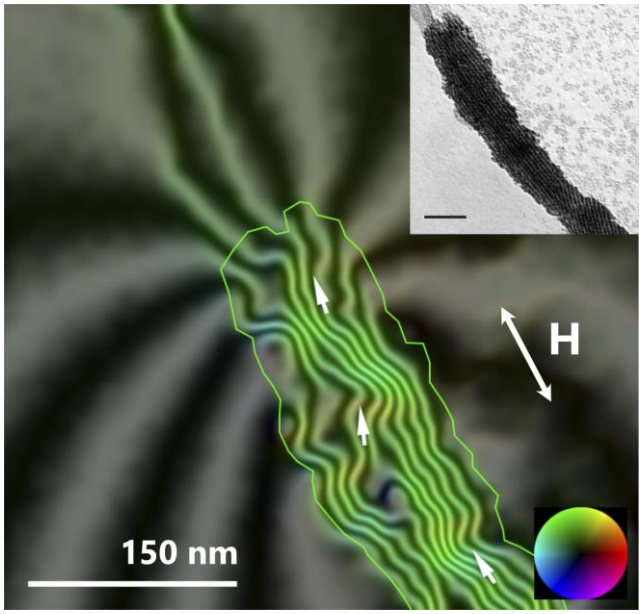

Figure S5: EH magnetic induction map of a double-gyroid nanowire formed by heterogenous nucleation at the border of graphene oxide and carbon layers (inset). The shape anisotropy of the wire produces a stray field, while the inner magnetic structure consists of small-angle domains. The contour lines and color coding indicate the magnetic field lines and their direction. The contour spacing is 2π/32 radians.

(d) Reproducibility and consistency of induction maps:

The magnetization switching experiments were performed several times. **Figure S6** shows two magnetic induction maps recorded from different switching cycles. Small differences between successive magnetic induction maps were observed. However, the main features are preserved between cycles, including field lines cutting across struts or surrounding vertices and the contour patterns in the double-gyroid region.

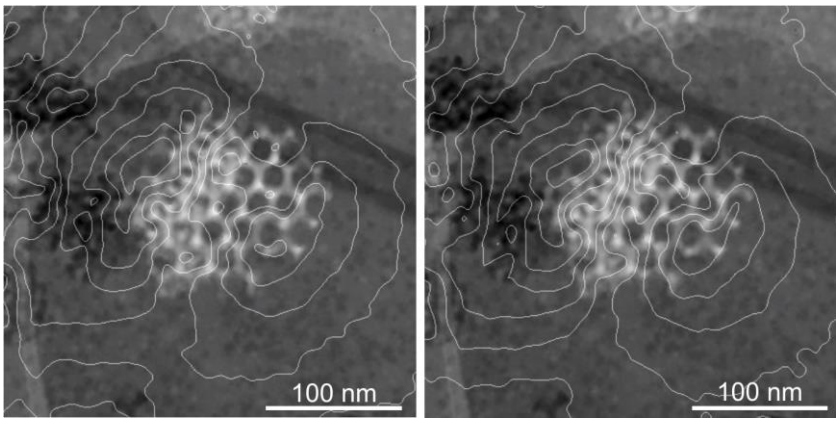

Figure S6: Magnetic induction maps recorded from a gyroid nanoparticle on a graphene oxide/carbon support during two successive switching experiments, showing small differences in recorded field. The field lines are superimposed on the mean inner potential contribution to the phase. The contour spacing is 0.1 radians.

Direct comparison of the experimental and simulated induction maps of the single/double gyroid shown in the Main Text in **Figure 3c** and **3d** and modelled in **Figure 4**, is not possible because the exact 3D structure of the gyroid nanoparticle is not known. However, the [111] viewing direction allows us to construct a model with a close resemblance to the real single/double gyroid nanoparticle and then use it to calculate the most probable magnetic state using finite-element micromagnetic simulations. Keeping this in mind, **Figure S7** shows the single/double gyroid nanoparticle and its experimentally determined induction map, side-by-side with the micromagnetic model and its calculated induction map.

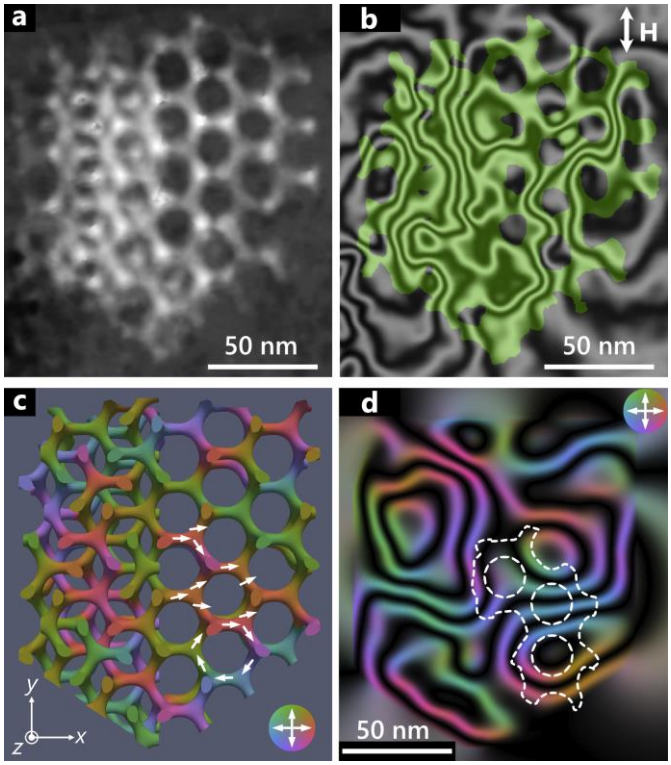

Figure S7: (a) The single/double-gyroid nanoparticle, (b) its experimental magnetic induction map, (c) micromagnetic model of the nanoparticle and (d) the calculated magnetic induction map. Note that in (b) a single green color is applied only to mask the nanoparticle. Color wheels in (c) and (d) show the direction of the in-plane magnetization and magnetic induction, respectively.

(e) Micromagnetic simulations:

Single-gyroid surfaces were generated in Mathematica® using the following equation:

$$\sin\left(\frac{2\pi x}{L}\right)\cos\left(\frac{2\pi y}{L}\right)+\sin\left(\frac{2\pi y}{L}\right)\cos\left(\frac{2\pi z}{L}\right)+\sin\left(\frac{2\pi z}{L}\right)\cos\left(\frac{2\pi x}{L}\right)=t \quad \text{(S1)}$$

where L is the unit cell length and the parameter t determines the volume fraction ϕ via the following relation:

$$2\phi = 101.5 - 68.1 \cdot t \quad \text{(S2)}$$

From previous experimental work, L was taken to be 42 nm and the volume fraction to be around 19 %, giving a value for t of 1.2. The gyroid geometries generated in Mathematica® were exported to the finite-element multiphysics program COMSOL® for removal of mesh defects and mesh refinement. The optimized single-/double-gyroid volume meshes were then imported into the GPU-accelerated TetraMag finite-element package.[4] Within TetraMag, the static magnetic configuration of the gyroid structure was calculated by solving numerically the Landau-Lifshitz-Gilbert equation of motion. Typical material parameters of permalloy, $\mu_0 M_S$ = 1 T and exchange constant A_S =1.3 × 10^{-11} J · m^{-1} were used. The magnetocrystalline anisotropy was neglected, therefore K_u = 0. The considered magnetic gyroid with dimensions of 4×5×1 unit cells was discretized into 69364 irregular tetrahedra with an average edge length of about 3 nm. The phenomenological Gilbert damping parameter α_G was set to 0.5 since we were only interested in the static magnetic configuration. Different initial magnetization distributions (both random and saturated along various unit cell vectors) were used to calculate the resulting remanent states.

References

(1) Scherer, M. R. J.; Cunha, P. M. S.; Steiner, U. Labyrinth-Induced Faceted Electrochemical Growth. Adv. Mater. **2014**, 26 (15), 2403–2407.

(2) Boothroyd, C.; Kovács, A.; Tillmann, K. FEI Titan G2 60-300 HOLO. *J. large-scale Res. Facil.* **2016**, *2*, A44.

(3) Saxton, W. O.; Pitt, T. J.; Horner, M. Digital Image Processing: The Semper System. *Ultramicroscopy* **1979**, *4* (3), 343–353.

(4) Kákay, A.; Westphal, E.; Hertel, R. Speedup of FEM Micromagnetic Simulations with Graphical Processing Units. IEEE Trans. Magn. **2010**, 46 (6), 2303–2306.